IEEE Access
Multidisciplinary | Rapid Review | Open Access Journal

Received 2 July 2023, accepted 8 August 2023, date of publication 14 August 2023, date of current version 17 August 2023.

Digital Object Identifier 10.1109/ACCESS.2023.3304750

RESEARCH ARTICLE

A Shared Aperture X/Ku-Band 5-Group-5-Element Series-Fed Center-Fed Antenna Array With Isolation Improvement for Airborne Synthetic Aperture Radar Applications

PRAVEENA KATI, (Graduate Student Member, IEEE), AND VENKATA KISHORE KOTHAPUDI, (Senior Member, IEEE)

Center of Excellence Advanced RF Microwave & Wireless Communications, Department of Electronics and Communication Engineering, School of Electrical, Electronics, and Communication Engineering, Vignan's Foundation for Science, Technology, and Research (VFSTR), Vadlamudi, Guntur, Andhra Pradesh 522213, India

Corresponding author: Venkata Kishore Kothapudi (v.k.kothapudi@ieee.org)

ABSTRACT This research paper introduces a novel dual-band single-polarized (DBSP) high gain shared aperture antenna (SAA) with better isolation is proposed for the use in Airborne Synthetic Aperture Radars (AIR-SARs). The SAA operating in both X-band and Ku-band with center frequencies of 9.3GHz (ideal for soil moisture estimation in agricultural areas) and 13.265GHz (suitable for applications in snow-covered regions, cold areas, and disaster monitoring) with a frequency ratio of 1:1.426. The SAA consists of four groups of 5-element series-fed center-fed planar array square microstrip patches for the X-band and one group of 5-element series-fed center-fed planar array square microstrip patches for the Ku-band. The inter-element spacing between patches is set at 0.7λ to meet the $\pm 25^0$ scan range requirements. To validate the antenna design, a prototype is fabricated and tested for S-parameters, radiation characteristics, and gain measurements. The antenna with return loss of S11 < -10 dB has an impedance bandwidth (BW) (9.1919-9.4674 GHz) (276 MHz with 2.96% BW) in X-band and (13.054-13.513 GHz) (459 MHz with 3.46% BW) in Ku-band. More than 25 dB of isolation has been measured between $S_{21} = S_{12}$ for case 3 and are >35dB isolation between in-band ports (P12/P23/P13) for case 4. Additionally, it achieves high gain values of 12.8 dBi for the X-band and 12 dBi for the Ku-band for case 3. The 2×2 planar array (5-elements in each group excited with coaxial probe feed) is connected with 8-way power divider (4-groups are feed with 4 power divider ports and other 4-ports are matched with 50Ω terminations) and achieved a gain of 19 dBi for the X-band and 12 dBi for the Ku-band for case 4. The combined gain is varied between 19dBi to 20dBi with 0^0 to 25^0 scan angle. The combined 2×2 planar x-band array Half-Power Beam width (HPBW) values are 16° in the E-plane and 12.6° in the H-plane for the X-band, while for the Ku-band, they are 22.7° in the E-plane and 78.4° in the H-plane. The antenna design shows a side-lobe level (SLL) of -16.2 dB at E-plane/$\varphi = 0^0$ for the X-band and -14.1 dB at E-plane/$\varphi = 0^0$ for the Ku-band. The size of the shared-aperture antenna is 160 mm × 160 mm × 1.6 mm. This paper presents the first reported SAA X/Ku-DBSP, which holds significant value for AIR-SAR applications. All the measured results were in line with simulated results and matched reasonably well.

INDEX TERMS Dual-band single-polarized aperture antenna, airborne synthetic aperture radar, dual frequency dual-polarization SAR.

The associate editor coordinating the review of this manuscript and approving it for publication was Hassan Tariq Chattha.

I. INTRODUCTION

Synthetic Aperture Radar (SAR) has been widely used for Earth remote sensing for more than 30 years [1]. AIR- SARs has been very useful over a wide range of applications, including sea and ice monitoring, mining, oil pollution monitoring, oceanography, snow monitoring, and classification of Earth terrain [3]. A prototype of a Dual-Frequency (C and X band) Dual-Linear Polarization Synthetic Aperture Radar (SAR) array antenna was developed, incorporating two interlaced arrays and their respective feed networks [2]. Researchers have conducted studies on series-fed square patch array antennas, which involve connecting half-wavelength patches of a standard resonator array antenna using $\lambda/2$ transmission lines [3]. One key advantage of series-fed antennas is their ability to provide equal aperture transfer and unidirectional radiation when all patches have the same width. Series-feed networks offer simplicity and compactness compared to corporate systems, enabling the implementation of low-loss feeding structures, as proposed by Pozar et al. [4]. The innovative microstrip series-fed tapered arrays demonstrate improved VSWR performance compared to conventional antenna arrays [5]. The utilization of a tapered design helps to reduce the side-lobe level in marine radar systems operating in the S, X, and Ku bands with an operating bandwidth of 9.3 to 9.4 GHz [6]. Recent developments in antenna technology have led to the development of coplanar proximity-coupled arrays and series-fed arrays. In particular, X-band 12 linear arrays have been designed, featuring direct coupling at 9.3 GHz and series feeding in the XZ and YZ planes [7]. It is necessary to achieve an isolation level better than 40 dB across the entire frequency band. These requirements are vital for accurate and reliable weather measurements, ensuring minimal interference and maximizing the antenna's performance in capturing relevant data [8]. A high-isolation dual-polarization microstrip patch antenna with omnidirectional radiation patterns has been proposed [9]. The antenna design achieved a wide impedance bandwidth, with the prototype-1 antenna providing an impedance bandwidth greater than 140 MHz (9.56-9.72 GHz) and the prototype-2 antenna achieving an impedance bandwidth of 140 MHz (9.58-9.74 GHz) for all individual ports [10]. The antenna design in [11] demonstrates impressive performance characteristics, including port isolation of 40 dB, cross-polarization of 20 dB. The L/S/X tri-band dual-polarization (TBDP) shared-aperture microstrip array antenna is designed for synthetic aperture radar (SAR) applications. It consists of two dual-band (L/S and L/X) dual-polarization shared-aperture sub-arrays and one L-band sub-array [12]. In the hybrid S-band feed architecture, linear and circular polarization characteristics of 2×2, 3×3, and 6×6 arrays have been tested. The antenna isolation between the elements is measured to be 45 dB for linear polarization and 43 dB for circular polarization has been achieved [13]. Circularly polarized magneto-electric dipole antenna arrays are employed in [14]. The dual-band antenna exhibits a gain of 8 dBi at 2.5 GHz. It also achieves 18 dB isolation between orthogonal ports within the S-band frequency range. In the X-band, with a measured gain of 11.5 dBi at 8 GHz and 28 dB measured isolation between orthogonal connections. The antenna effectively isolates both frequency bands with a minimum of 38 dB separation. The gain of the S-band antenna measures at 7.5 dBi, while the X-band antenna achieves a gain of 10.5 dBi [15], [16]. In [17], the design provides a gain of 8 dBi at the center frequency of 2.5 GHz and ensures a high level of isolation, measuring 18 dB between orthogonal ports within the S-band. For the X-band, it achieves a gain of 11.5 dBi at the center frequency of 8 GHz and maintains a significant isolation of 28 dB between orthogonal ports specifically designed for the X-band. In [18], by utilizing electromagnetic coupling (EMCP), the antennas exhibit high isolation between perpendicular ports, surpassing 28 dB at frequencies of 2.5 GHz and 8.2 GHz. With a gain of 7.4 dBi at 2.5 GHz and 10 dBi at 8 GHz, these satellite antennas are capable of accurately tracking, monitoring, and commanding operations [18]. The planar antenna array demonstrates accuracy bandwidths of 3.6% in the X-band, 6.7% in the Ku-band, and 5.3% in the Ka-band [19]. A Metamaterial-Based *S*/*X*-Band Shared-Aperture Phased-Array Antenna frequency ratio of 2.7:1 having a multilayer configuration with a gain of 7.6dBi with scan angle $\pm 50°$ is implemented in [32]. A 2-layer Ku/Ka band with frequency ratio of 2.1 by using Structure-Reuse Technique has been implemented <9dBi gain having an array size of $2 \times 3.4 \times 4$ is implemented in [31]. A Bifunctional Meta surface technique with shared aperture concept was introduced in [30] with a FR of 2.4 at S/C-band having again of 7.9dBi and 2.7dBi. An SAA with single and dual polarization has been implemented with Ku/Ka-band with an isolation of 30dB in [33]. A 2D SAA with Ku- and Ka-Band multilayer 8×8 array has been implemented with again of 22dBi at booth the bands with an isolation of 30dB in [34]. An SAA with radiation pattern distortion technique has been implemented with FR of 2.1 has been achieved with multilayer configuration with a gain of 7.3/13DBi at both S/L-bands in [35]. In [36], An SAA with high Highly-Isolated RF Power and Information Receiving System Based on Dual-Band Dual-Circular-Polarized Shared-Aperture Antenna. In [37], An SAA with cavity Slot Antenna-in-Package with Enhanced Beam Coverage for MIMO applications has been implemented. In [38], An SAA with dual band multi polarization at Ku-/Ka-band for Satellite Communication with a gain of 18dBi/23.4dBi and isolation of 15dB has been implemented. In [39], K-/Ka-Band Shared-Aperture Phased Array gain of 4.5dBi and isolation of 40dB was achieved.

The works reported in the present SAA design, have many advantages like: 1) Low cost and low profile (single layer PCB); 2) Efficient utilization of physical aperture; Single-layer PCB features array segmentation, and gain enhancement with power divider/combiner (20dBi/13dBi at X/Ku-bands) (it's a drawback in multilayer SAA technology);

3)series-fed design to reduce the microstrip transmission line losses; 4) Minimized aperture size 160mm 160mm 1.6mm (Almost 250mm 250mm 15mm in multilayer SAA); 5)design provides four groups of X-band 5-element series- fed arrays, one of the groups can be used as TX and other can be used as Rx; 6) Passive phased array system. 7) Inter-element spacing of 0.7 free space wavelengths allows less number of elements with required directivity and beam width and provides a scanning capability of $\pm 25^0$ which allows grating lobe free scanning. All of these advantages make it ideal for present SAA design. The specifications and design goals of this work are summarized in table 1.

This paper is organized accordingly. Section II presents the synthetic aperture radar, section III presents design specifications and section IV presents SAA design configuration and case wise design analysis. Section V presents simulated and measured results analysis of X/Ku-band, section VI presents directions of improvement and finally section VII presents conclusions of the proposed research work.

II. SYNTHETIC APERTURE RADAR

SAR technology operates across a frequency range spanning from Very High Frequency (VHF) to Terahertz (THz). Lower frequencies are advantageous for better penetration through weather, vegetation, and the ground, while higher frequencies enable the capture of finer details in the resulting images [20]. SAR is also employed in snow tracking, particularly in regions with significant snowfall. Their applications encompass monitoring sea and ice, detecting oil pollution, supporting meteorological studies, tracking snow dynamics, and facilitating terrain classification [1], [21], [22], [23], [24], [25]. SAR systems are designed with a side-looking imaging geometry and employ pulsed radar technology on a forward-moving platform [26]. As the SAR platform travels along a linear trajectory above a reference point, it emits high-frequency microwave pulses towards the antenna's illuminating area and captures the resulting echoes reflected from the Earth's surface. This arrangement involves incorporating a 'two-way signal time delay' and 'pulse number' to properly position the echoes within the array, enabling subsequent analysis and interpretation of the SAR data [27]. These techniques and features in civil-use SAR systems contribute to advancements in SAR imaging quality, data analysis, and the extraction of valuable information for a wide range of applications [28]. Starting in 2003, several satellite missions initiated the delivery of multi-mode Synthetic Aperture Radar (SAR) data across different frequency bands. These missions include COSMO-Sky Med, ALMAZ-1, Radarsat-2 (C-band), Sea salt, JERS-1, Terra SAR-X, and Tan DEM-X (X-band), along with Radarsat-2 (C-band). Among them, Terra SAR-X, Tan DEM-X, COSMO-Sky Med, and Radarsat-2 operate in the X-band, while Radarsat-1, ERS-1, and ERS-2 primarily utilize the C-band. These satellites have been instrumental in providing SAR data, enabling a wide range of applications. By leveraging radar technology, these missions have significantly contributed to various fields such as Earth observation, environmental monitoring, disaster management, and mapping. [29].

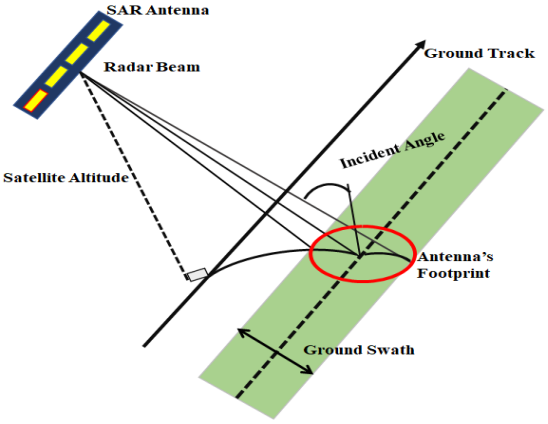

FIGURE 1. Airborne synthetic aperture radar geometry.

TABLE 1. X/Ku-band single-layer shared aperture antenna specifications.

Operation bands	X-band	Ku-band
Center frequency	9.3 GHz	13.265 GHz
Polarization	Linear	Linear
Impedance bandwidth	>200 MHz	>200 MHz
Antenna size	160 x 160 x 1.6 mm^3	
Radiation efficiency	80%	80%
Gain	>20 dBi	>12dBi
Cross polarization	>-25	>-25
Isolation	>25	>25
Side Lobe Level	-15dB	-15dB
Scan Range	$\pm 25^0$	$\pm 25^0$
Inter-element Spacing	0.7λ	0.7λ

III. SAA DESIGN SPECIFICATIONS

The given specifications in Table-1 outline the requirements for the single-polarized X-band and Ku-band SAA (Synthetic Aperture Radar) operations. The X-band operates at a frequency of 9.3 GHz, while the Ku-band operates at 13.265 GHz. In both bands, it is essential to maintain a bandwidth of >200MHz. The expected polarization for both bands is linear. To ensure proper functionality, the isolation between ports must exceed 25 dB. Additionally, the antenna should exhibit low cross-polarization, with a minimum of -25 dB. These specifications have been carefully chosen to meet the specific needs of the Airborne SAR application. The choice of beam patterns has been guided by the requirements of this application. Airborne Synthetic Aperture Radar Geometry as shown in Figure-1.

IV. SAA DESIGN CONFIGURATION

A. CASE-1: X-BAND 5-ELEMENT DESIGN

In Figure 2(a), the X-band first group patch is depicted with five orthogonal elements that have linearly aligned antenna

physical parameters. To achieve linear polarization, the patch is excited using a 50 Ω direct-coupled coaxial feeding. In order to achieve impedance matching, a direct-coupled coaxial feed matching transformer is utilized with a 12-mm series feed length and 1.5-mm width. The X-band antenna, which consists of a 5-element planar array, is designed with a single port (coaxial probe). The implementation of a coaxial feed helps improve the impedance characteristics of the proposed antenna. To calculate the element distance in the X-band Square Array Antenna (SAA) square distribution, Equations (1) and (2) can be utilized.

$$d_{xX} = \frac{\lambda vX}{1 + \sin\theta x} \tag{1}$$

$$d_{yX} = \frac{\lambda_{HX}}{1 + \sin\theta_y} \tag{2}$$

Table 2 presents the optimized parameters for the X-band element, which consists of a 12 mm series feed length, a guided wavelength (λg) of 21.7 mm at 9.3 GHz, and a 1.6 mm series feed width. The frequency response of the X-band elements of S-parameter and gain depicted in Figure 2(c). The antenna exhibits resonance at 9.3 GHz with a single-port S11 value of -19 dB. The impedance bandwidth spans from 9.1919 GHz to 9.4674 GHz, equivalent to 275.5 MHz, while maintaining $|S11| < -10$ dB and $|S21| < -50$ dB. Figure 2(b) showcases the surface current distribution, providing insights into the polarization of the S11 port.

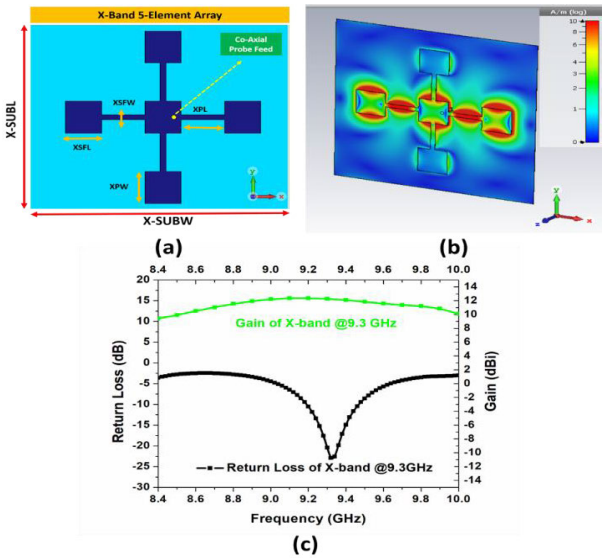

FIGURE 2. a)Geometry of X-band b) Surface current distribution for X-band c) Return loss and gain vs frequency for X-band.

B. CASE-2: KU-BAND 5-ELEMENT DESIGN

Figure 3 illustrates the physical characteristics of a 5-element single-group antenna designed for linear polarization in the Ku-band. The antenna is excited using a 50 Ω direct-coupled coaxial feeding, with impedance matching achieved through a 9 mm length and 1.2 mm width matching transformer. Table 2 presents the parameter values specific to the X/Ku-SAA unit

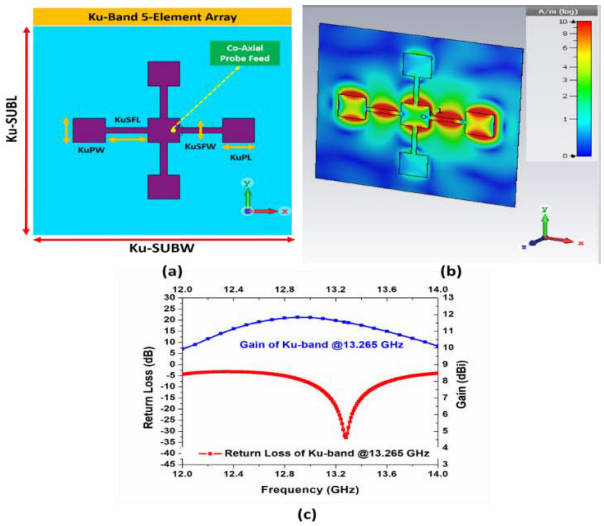

FIGURE 3. a) Geometry of Ku-Band b) Surface current distribution for Ku-band c) Return loss and gain vs frequency for Ku-band.

TABLE 2. X/Ku-SAA unit Parameters for Ku-Band (Optimized).

Parameter	XL	XW	XSFL	XSFW
Value mm)	10	10	12	1.6
Vale(λ_0)	0.31	0.31	0.372	0.049
Value(λg)	0.46	0.46	0.55	0.073
λ0: Free space wavelength concerning the velocity of propagation in air center frequency (9.3GHz) (0.0322 meters) **λg**: Guided wavelength concerning the velocity of propagation in substrate material (RT-Duroid-5880) (0.0217 meters)				
Parameter	**Ku L**	**Ku W**	**Ku SFL**	**Ku SFW**
Value (mm)	7	7	9	1.2
Vale(λ_0)	0.309	0.309	0.398	0.053
Value(λg)	0.449	0.449	0.577	0.076
λ0: Free space wavelength concerning the velocity of propagation in air center frequency (13.265GHz) (0.0226 meters), **λg**: Guided wavelength concerning the velocity of propagation in substrate material (RT-Duroid-5880) (0.0217 meters)				

in the Ku-band, while Equations (1) and (2) are used to calculate the element distance on the X and Y-axes of the Ku-band SAA. The optimized Ku-band element parameters are provided in Table 2, and Figure 3(a) depicts the ideal configuration with a 9 mm series feed length, a guided wavelength of 15.59 mm at 13.265 GHz, and a series feed width of 1.6 mm at 9.3 GHz. The frequency response of the Ku-band elements of return loss and gain shown in Figure 3(c), resonating at 13.265 GHz at port S11, while Figure 3(b) displays the surface current distribution of the S11 port.

C. CASE-3: GEOMETRY CONFIGURATIONS OF A SINGLE GROUP OF X-BAND AND Ku-BAND SAA

Figure 4(a) depicts the geometry configurations of the proposed X/Ku-band single element for X-band and Ku-Band SAA and shows the evolution stages. The array consists of

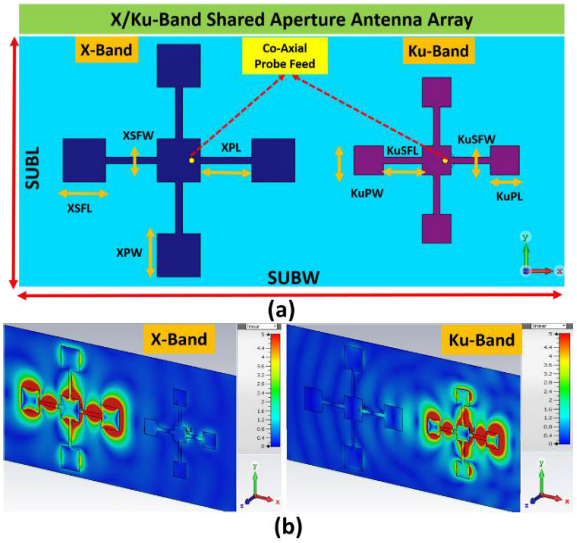

FIGURE 4. (a) X/Ku-band shared aperture antenna geometry; (b) Surface current distribution for X-band and ku-band shared aperture antenna array.

5 identical group elements arranged in a series-fed configuration, with both vertical and horizontal planes containing three-element groups. The X-band array utilizes a series-fed design with an optimized feed width (SFW) of 1.6 mm. For the X-band array, the inter-element spacing is typically chosen to be around 0.7λ, corresponding to a center frequency of 9.3 GHz (approximately one guided wavelength). In this specific SAA X-band antenna, the inter-element spacing (SFL) is set at 12 mm. This optimal spacing allows for a narrower beam width and improved directivity while minimizing the number of antenna elements required. Similarly, in the SAA Ku-band linear array, the element spacing is set at 0.7λ, which corresponds to a resonance frequency of 13.265 GHz (approximately one guided wavelength).

The design process for the entire system utilizes CST software, a full-wave electromagnetic solver. Figures 4(a) provide a visual representation of the design parameters, showcasing the geometry view of the X-band and Ku-band arrays, as well as the surface current distribution, respectively. Regarding the propagation velocity, the overall size of the X/Ku-DBSP SAA is $120 \times 60 \times 1.6\ \text{mm}^3$, indicating its compact form. The proposed SAA mutual coupling effect on both transmitting and receiving modes, antenna elements must be calculated to detect estimations of arrival, accuracy, and resolution. The isolation of the antenna depends on the correct calculation of current distribution on the complete body of the SAA, computing the SCD shown in Figure 4(b) takes the mutual coupling effect into account. Boundary conditions are not needed to be specified to reduce complexity and processing time. The presence of a mutual coupling effect in an antenna receiver relies on correctly calculating the current distribution across the entire antenna structure. In order to account for the mutual coupling effect, the computation of the surface current distribution, as depicted in Figure 4(b), takes this factor into consideration. The scattering matrix of X/Ku-band is given in matrix format by representing returnloss and isolation for all the ports for case 3 and case 4 as given below.

TABLE 3. Specifications of the proposed substrate material.

Substrate Material (RT/Duroid-5880) (L × W × H)							
Parameter	*L*	*W*	*H*	Parameter	*L*	*W*	*H*
Value (mm)	160	160	1.6	Value (mm)	160	160	1.6
Value ($\lambda 0$) @9.3 GHz	3.72	1.863	0.049	Value ($\lambda 0$) @13.265 GHz	5.309	2.654	0.07707
Value (λg) @13.265 GHz	5.529	2.764	0.073	Value (λg) @13.265 GHz	7.697	3.848	0.102
mm: millimeter; *L*: Length; *W*: Width; *H*: Height.							

$$\begin{bmatrix} S11 & S12 \\ S21 & S22 \end{bmatrix} \rightarrow \begin{bmatrix} -23.4 & -28.8 \\ -28.8 & -32.9 \end{bmatrix} \quad \text{Case-3}$$

$$\begin{bmatrix} S11 & S12 & S13 & S14 & S15 \\ S21 & S22 & S23 & S24 & S25 \\ S31 & S32 & S33 & S34 & S35 \\ S41 & S42 & S43 & S44 & S45 \\ S51 & S52 & S53 & S54 & S55 \end{bmatrix} \rightarrow \begin{bmatrix} -19.8 & -61.2 & -59.7 & -67.0 & -47.0 \\ -61.2 & -19.8 & -67.2 & -61.4 & -52.4 \\ -59.7 & -67.1 & -19.8 & -61.7 & -47.1 \\ -67.0 & -61.4 & -61.7 & -19.8 & -52.4 \\ -47.0 & -52.4 & -47.1 & -52.4 & -22.2 \end{bmatrix} \quad \text{Case-4}$$

D. CASE-4: GEOMETRY AND CONFIGURATION AT 4- GROUPS (X-BAND) AND FIFTH GROUP (Ku-BAND) FOR X/Ku-BAND- SAA

The X-band and Ku-band SAA configurations employ a single-layer design to achieve linear polarization with a frequency ratio of 1:1.426. Figure 5 provides a top view, illustrating a common aperture with 2×2 planar square patch antenna array consisting of 4 groups. To enhance gain, narrow the beamwidth, and ensure port isolation, both antennas are positioned on top of the substrate for the X-band and in the middle for the Ku-band. The antennas utilize microstrip patch and series feed, employing coaxial probe feeding for the X/Ku-band SAA. The RT/Duroid 5880 substrate material [40], is used to support the design and fabrication with a loss tangent of 0.0009 and a relative dielectric constant of 2.2, resulting in the overall size of the X/Ku-DBSP SAA of $160 \times 160 \times 1.6\ \text{mm}^3$ and are tabuleted in table 3. This corresponds to $3.72 \times 3.72 \times 0.049\ \lambda_0$ with respect to the propagation velocity in the air, or $5.329 \times 2.764 \times 0.073\ \lambda_9$ with respect to the propagation velocity in the substrate material, aligning with the X-band center frequency of 9.3 GHz, or $7.697 \times 3.848 \times 0.102\ \lambda_9$ for the Ku-band center frequency of 13.265 GHz. All simulations were conducted using CST Microwave Studio 2016 [41], and FIT-Finite Integration Technique based on the FDTD-Finite Difference Time Domain simulation program. The SAA design incorporates both bands into a compact area to enable frequency diversity. The antenna design employs a high X/Ku-band frequency

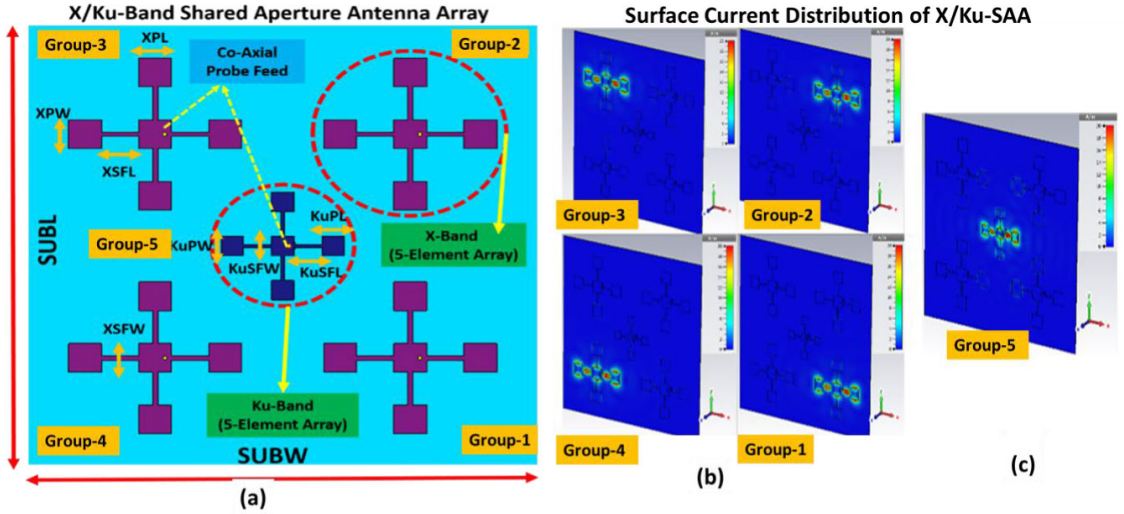

FIGURE 5. (a) The geometry of the configuration with optimized dimensions of 2 × 2 planar array (SAA). (b) Surface current distribution for X-band (4-Groups); (c) Surface current distribution for Ku-band (single group).

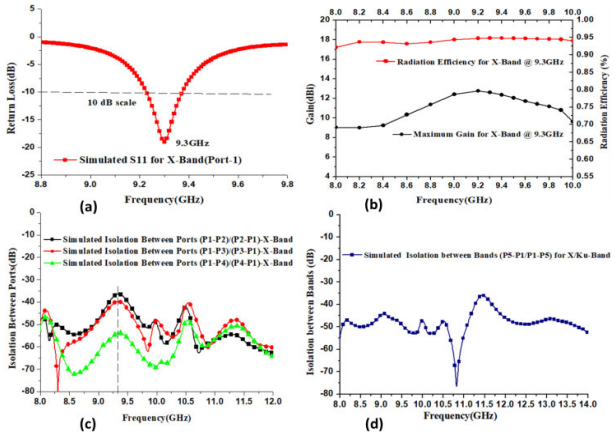

FIGURE 6. (a) : Simulated return Loss for X-band (b) Simulated gain vs frequency for X-band (c) Simulated isolation between Port1-Port4 (d) Simulated isolation between Port-(5,1).

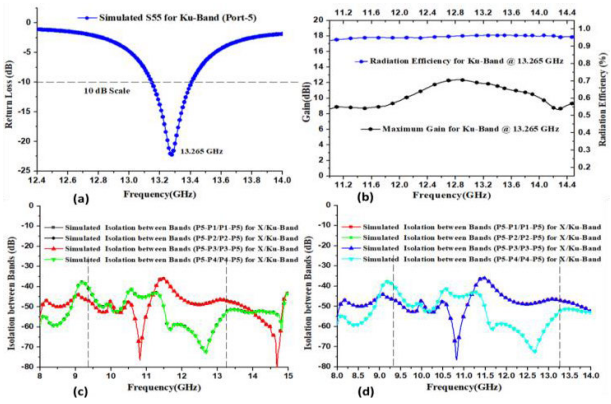

FIGURE 7. (a) : Simulated return loss for X-band (b) Simulated gain vs frequency for X-band (c) Simulated isolation between Port1-Port5 (d) Simulated isolation between Ports-(5,1)-(5,2)-(5,3)-(5,4).

ratio, a 4-group 5-element planar array, and a 5-element single-group in the middle with a series feed and center feed of five ports. Series feeding allows the fabrication of the antenna on the same substrate, reducing production complexity and costs. By combining the radiating components of both bands within the same aperture, it is essential to investigate the current radiating patch distribution. Figure 5(b & c) displays the current distribution of the propagating components at the respective frequencies, demonstrating that at 9.3 GHz in the X-band operation, the cross-patches are stimulated while the apertures remain passive, as shown in Figure 6(c). The current distribution analysis reveals minimal mutual interaction between the antenna array elements at the two bands, confirming that the antenna operates independently in the X and Ku bands. Figure-6(a)-(d) and Figure 7(a)-(d) show casing of simulated return Loss, gain, radiation efficiency, isolation between the X-band ports and isolation between X- and Ku-bands. Simulated Isolation between Port-1 to Port-5 (d) Simulated Isolation between Port-1 to Port-5. From the Figure-6(a)-(d) and 7(a)-(d) it is observed that the antenna with return loss of S11 < -10 dB has an impedance bandwidth (BW) (9.1919-9.4674 GHz) (275 MHz with 2.96% BW) in X-band and (13.054-13.513 GHz) (459 MHz with 3.46% BW) in Ku-band. More than 25 dB of isolation has been observed between the bands and ports for case 4 and are >35dB isolation between in-band ports (P12/P23/P13) for case 4. Additionally, it achieves high gain values of 12.8 dBi for the X-band (Port-1) and 12 dBi for the Ku-band (Port-5) for case 4. All remaining ports i.e P2, P3, and P4 also having similar performance and has been given in Table 4.

V. SIMULATED AND MEASURED RESULTS ANALYSIS FOR X/Ku-SAA

The X/Ku-band shared-aperture antenna array prototype, with central frequencies of 9.3 GHz and 13.265 GHz for

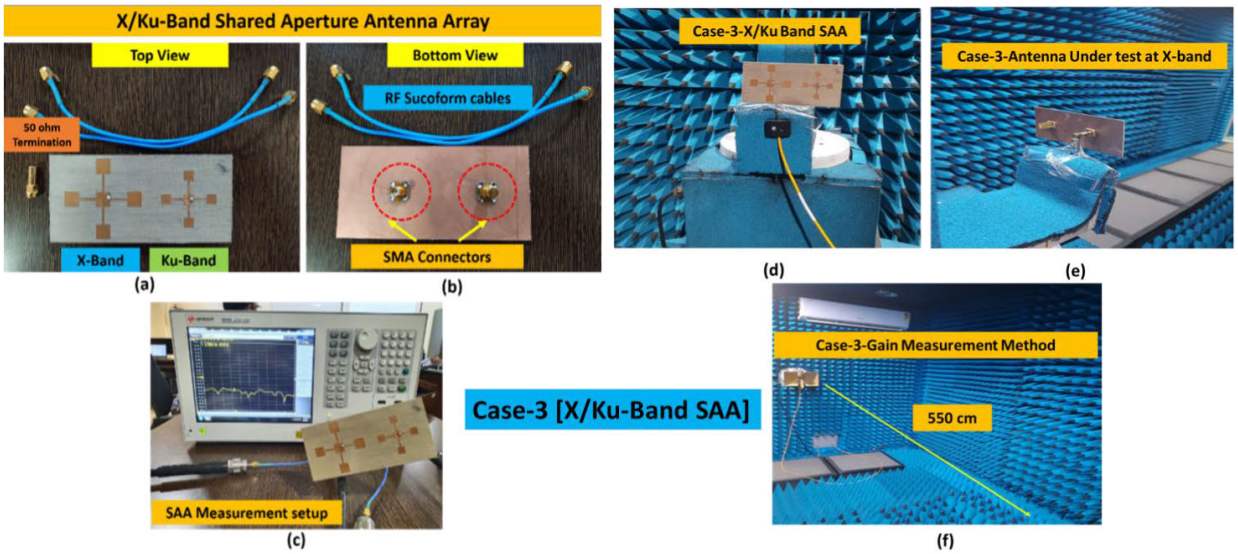

FIGURE 8. Fabricated and measurement results prototype of case-3 (a) Top view of X/Ku-band SAA array (b) Bottom view of X/Ku-band SAA (c) Measurement setup with VNA (d) Measurement setup in anechoic chamber for X-band (e)Measurement setup in anechoic chamber for Ku-Band (f) Measurement setup using standard horn gain.

X- and Ku-bands, respectively, are fabricated and measured to validate the design for both case-3 and case-4. As shown in Figure 8 (a-f), the prototype array is incorporated with X/Ku-bands. The top and bottom views of X/Ku band SAA is shown in figure 8(a & b). The *S*-parameters and radiation patterns are measured using Keysight-E5063A (100 KHz-14 KHz) ENA Series Network Analyzer as shown in Figure 8(c), and the radiation patterns and gain measurements are measured in an anechoic chamber. The measurement setups for both *S*-parameters and radiation patterns are shown in Figures 4(c-f). The X/Ku-band SAA is fabricated and experimentally verified. Similarly Figure 14 presents the SAA prototype measurement set-up, top view and bottom view of 2×2 X-band planar array with Ku-band 5-element array. The measurement setup of 4-groups of 5-element X-band array and Ku-band 5-element array for both *S*-parameters and radiation patterns are shown in Figures 14(c-f). Figure 20(a-d) presents the combined ports with two-way power combiner/dividers for maximum combined X-band gain with linear polarization. The notations of excitation port denotes X-band port (port-1) and Ku-band (port-2) for case 3. The notations of ports for case 4 are X-band group-1 as port-1, Group 2 as port-2, group 3 as port-3, group 4 as port-4, and finally group 5 i.e Ku-band 5-element array excitation port as port-5. Following subsections deals with case-3 and case-4 along with each port excitations individually.

A. CASE 3

1) PORT-1 EXCITED (X-BAND@9.3 GHz)

Figure 9 shows the comparison between the simulated and measured S-parameters of the proposed SAA at X/Ku-band antenna. For port-1 the simulated return loss bandwidth S11

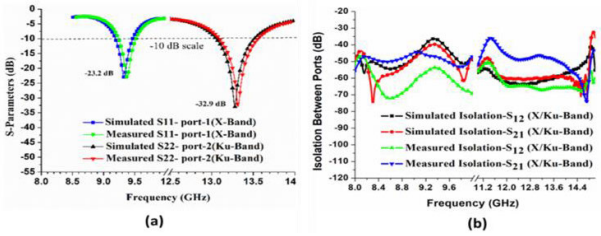

FIGURE 9. Simulated and measured return loss of S11 and S22 for X/Ku-Band SAA. (b) Simulated and measured.

Simulated and measured experimental S-parameters (S_{11}) of X/Ku-band shown in Figure-9(a), Simulated and measured Isolation between bands that port-1 (P1) and port-2 (P2) ($|S_{12}| = |S_{21}|$) shown in Figure-9(b), the return loss results show a -10dB bandwidth at port-1 S_{11} and port-2 S_{22}, X-band ranging from 9.1919-9.4674 GHz. Isolation results between X/Ku-band over 48 dB.

Figure 7 (a-b) shows the simulated and measured X-band radiation pattern at 9.3 GHz. The antenna radiates well on the broadside. A 50 load on port 1 (X-band linear polarization) gives P1 a half-power beam width of 78.5^0 and a 12.3 dBi gain. A half-power beam width of 23.4^0 and a gain of 12 dBi are observed in the E-plane. In the H-planes, the observed SLL are under -16.2 dB and cross-pol levels are -30 dB (E-Plane), -21.7 dB (H-Plane). Both planes have an FTBR of 18 dB or higher.

2) PORT-2 EXCITED (Ku-BAND@13.265 GHz)

Figure 9 shows the comparison between the simulated and measured S-parameters of the proposed SAA at X/Ku-band antenna. For port-2 the simulated return loss bandwidth S11

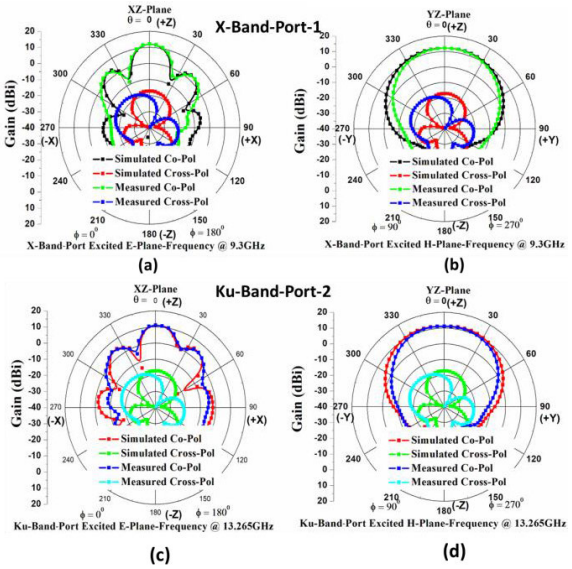

FIGURE 10. Simulated & measured far-field radiation characteristics of X-band 5-element array@ 9.3 GHz (a) XZ-Plane (E-Plane) (b) YZ-Plane (H-Plane) and simulated & Measured far-field radiation characteristics of Ku-Band 5-element array@ 13.265 GHz (c) XZ-Plane (E-Plane) (d) YZ-Plane (H-Plane).

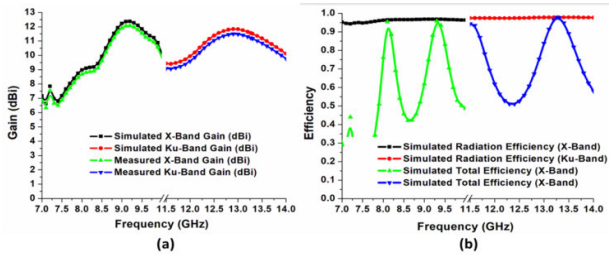

FIGURE 11. (a) Simulated and measured gain and (b) Simulated radiation efficiency of X/Ku-Band.

Simulated and measured experimental S-parameters (S_{11}) of X/Ku-band shown in Figure-9(a), Simulated and measured isolation between bands that port-1 (P1) and port-2 (P2) ($|S_{12}| = |S_{21}|$) shown in Figure-9(b), the return loss results show a -10dB bandwidth at port-2 S_{22} Ku-band ranging from 13.054-13.513 GHz. Isolation results between X/Ku-band over 48 dB.

Figure 10 (a-b) shows the simulated and measured experimental Ku-band antenna radiation pattern at 13.265 GHz. The antenna has good HPBW and gains due to the increase in electrical size at high-band. The P1 is terminated with a 50 load for Ku-band linear polarization (P2). The antenna's HPBW is 20.1^0 and its gain is 11.3 dBi. The HPBW is 76.6^0 and the gain is 11.3 dBi. In the H-planes, SLL is -14.1 dB. The cross-pol is below -29 dB in the E and H planes at 13.265 GHz. FTBR > 18 dB in both planes.

A standard gain is utilized as a reference antenna during the measurement of the gains. Figure 11 shows the simulated realized gains of this antenna. Peak gain is 12.3 dBi at 9.3 GHz, equivalent to efficiencies of 93/92 %.

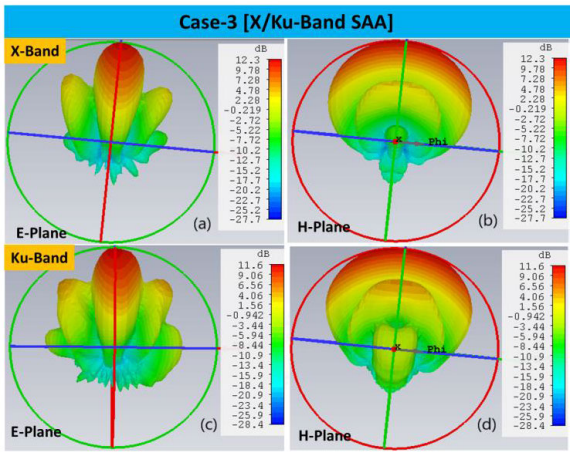

FIGURE 12. 3D radiation patterns of single-layer SAA design configuration at X/Ku-Band (a) X-band- E-Plane, (b) X-band-H-Plane, (c) Ku-Band-E-Plane and (d) Ku-Band-H-Plane.

In the Ku-band, maximal linear polarization gains are around 11.6 dBi at 13.265 GHz, equivalent to efficiencies of 94 % and 92%. Figure 12 depicts 3D radiation patterns. The X/Ku-band SAA S-parameters and radiation properties such as bandwidth, gain radiation efficiency, SLL, HPBW, and cross-pol, are determined and summarized in Table-4

B. CASE 4

1) PORT-1 EXCITED (P2-P3-P4 MATCHED WITH 50ω TERMINATIONS) (X-BAND@9.3 GHz) AND PORT-2 EXCITED Ku-BAND @13.265GHz

Figure 13 presents the SAA prototype measurement set-up, top view and bottom view of 2 × 2 X-band planar array with Ku-band 5-element array. The measurement setup of 4-groups of 5-element X-band array and Ku-band 5-element array for both *S*-parameters and gain, radiation characteristics of X/Ku-SAA and 3D patterns are shown in Figures 14 (a-b), 15(a-c), 16(a-d), 17(a-d), 18(a-b), 19(a-e). The notation of P1 refers to the group-1 of the X-band and P2 refers to the group-2 of the X-band and P3 refers to the group-3 of the X-band, P4 refers to the group-4 of the X-band. A good agreement between measured and simulated results was observed, with a bandwidth (BW) of 10 dB at port-1 (P1), port-2 (P2), port-3 (P3) and port-4 (P4) ranging from (9.1919-9.4674 GHz) (275 MHz with 2.96% BW) in X-band and (13.054-13.513 GHz) (459 MHz with 3.46% BW) in Ku-band are shown in Figure 16 (a). More than 25 dB of isolation has been observed between the bands and ports for case 4 and are >35dB isolation between in-band ports (P12/P23/P13) for case 4 are shown in Figure 15 (a)-(c) Additionally, it achieves high gain values of 12.8 dBi for the X-band (Port-1,2,3,4) and 12 dBi for the Ku-band (Port-5) for case 4 are shown inf Figure 14(b). All remaining ports i.e P2, P3, and P4 also having similar performance and has been given in Table 4. Figure 16-18 shows the polar radiation patterns for all excitation ports i.e X-band

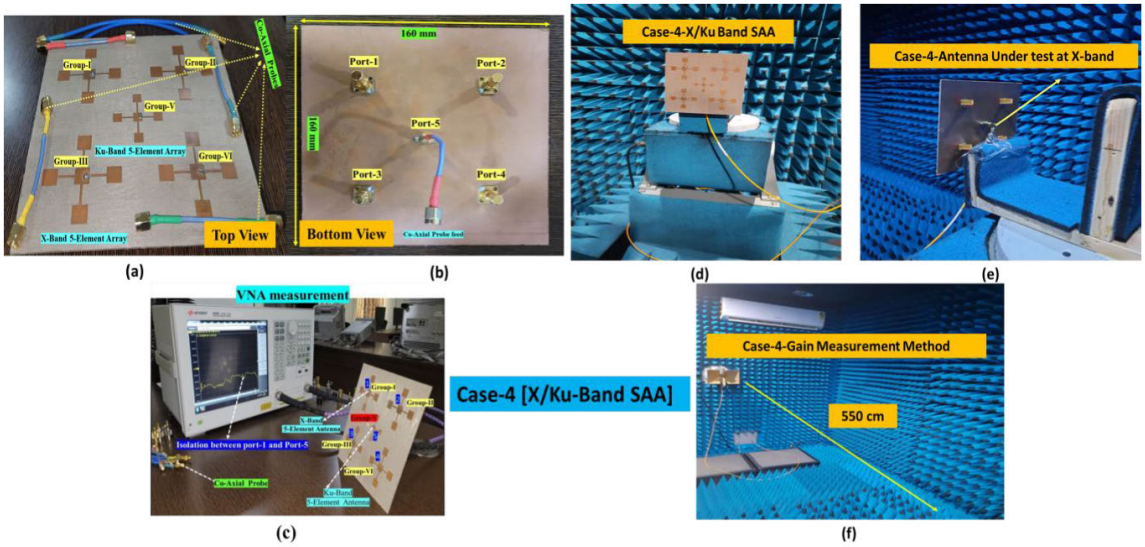

FIGURE 13. Fabricated and measurement results prototype of case-4 (a) Top view of X/Ku-band SAA Array (b) Bottom view of X/Ku-Band SAA (c) Measurement setup with VNA (d) Measurement setup in anechoic chamber for X-band (e)Measurement setup in anechoic chamber for Ku-band (f) Measurement setup using standard horn gain.

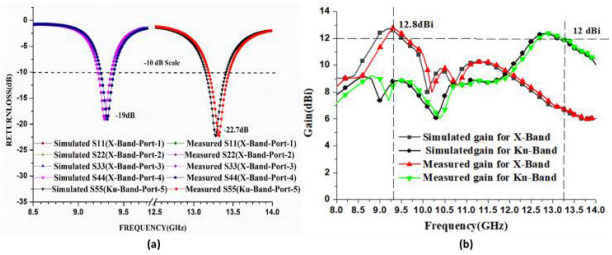

FIGURE 14. (a) Simulated and measured return loss for S-parameters (S11,S22,S33,S44 and S55) for X/Ku-Band (b) Simulated and measured gain vs frequency for SAA.

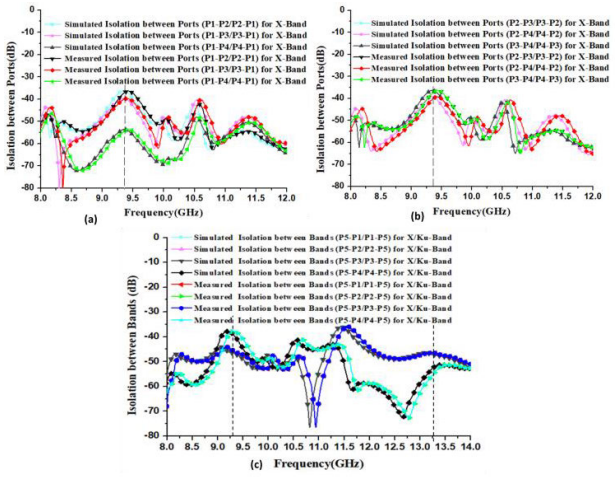

FIGURE 15. (a) Simulated and measured isolation between ports (1,2) (1,3) and (1,4) for X/ku-band. (b) Simulated and measured isolation between ports (2,3) (2,4) and (3,4) for X/ku-band.(c) Simulated and measured isolation between ports (5,1) (5,2) (5,3) and (5,4) for X/Ku-band.

(P1, P2, P3, and P4) and Ku-band (P5) and results were presented in table 4. Figure 19(a-e) shows the 3D radiation patterns of X/Ku-band SAA.

2) POWER DIVIDER/COMBINER PORT IS EXCITED (X-BAND@9.3 GHz) AND PORT-2 EXCITED WHEN X-BAND GROUPS COMBINED (Ku-BAND@13.265 GHz)

Figure 20(a-d) shows the X/Ku-band SAA at 9.3 GHz when power divider/combiner port is excited and P5 (Ku-band) is terminated with a 50 Ω matched load. The experimental results are in good agreement with the simulations, showing better scattering and linear polarization characteristics with better gain and narrow beam width.

Figure 21(a-b) shows the simulated and measured radiation patterns of the X-band combined array using power divider/combiner and Ku-band 5-element array at 9.3 GHz and 13.265 GHz. In the experiment, the SLLs are below -15dB. The measured cross-pol is higher than 25 dB. The measured gain of X-band array at 9.3GHz is 19 dBi and the radiation efficiency is about 90%. For the X-band design, the half-power beamwidth (HPBW) is 16°/12.1° for the E/H-planes. For Ku-band similar characteristics has been observed as discussed in case-3 and case-4.

3) BEAM SCANNING MECHANISM FOR X-BAND @9.3 GHz

The beam scanning capability of the combined four-port 2 × 2 planar array configuration is achieved by applying different excitation phase values to the four input ports for linear polarization, along with a 4-way power divider to maximize gain. To study the beam scanning capability, the initial configuration involves exciting all ports with a zero-degree phase and equal amplitude. Figure-22 Scan angle patterns for different progressive phase shift, Figure-22(a) X-band E-plane. Figure-22(b) X-band H-plane.

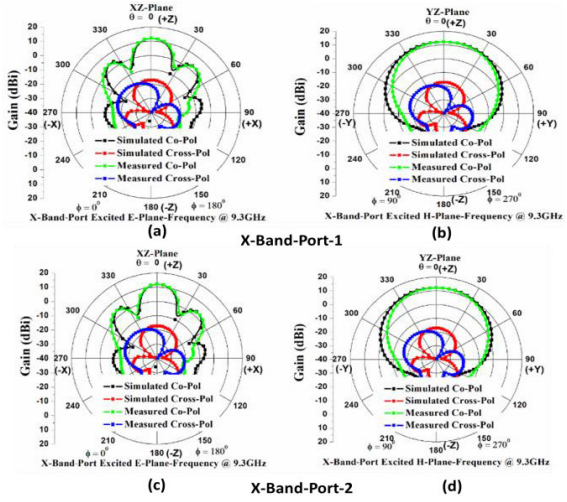

FIGURE 16. Simulated and measured polar plots of single-layer SAA design configuration at X- Band @ port-1 and Port-2 (a) E-Plane, (b) H-Plane.

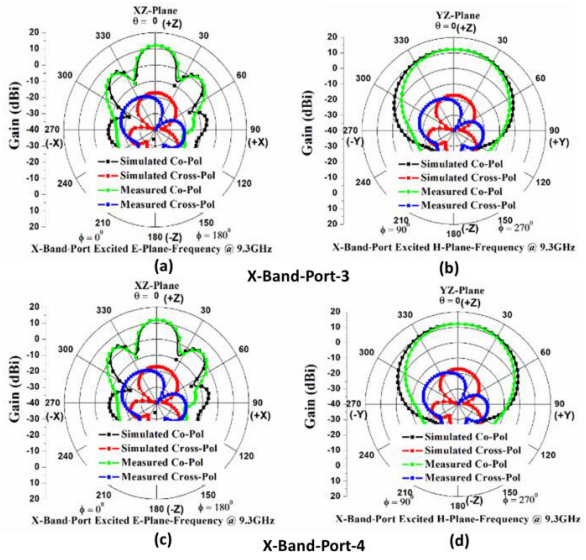

FIGURE 17. Simulated and measured polar plots of single-layer SAA design configuration at X- Band @ port-3 and Port-4 (a) E-Plane, (b) H-Plane.

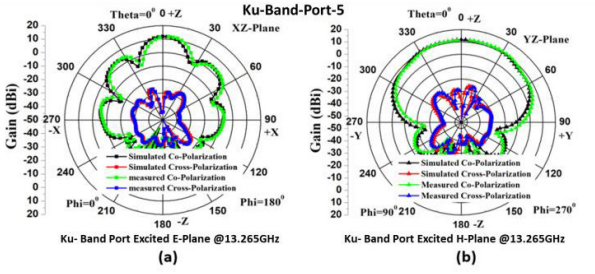

FIGURE 18. Simulated and measured polar plots of Single-layer SAA design configuration at Ku-Band @ port-5(a) E-Plane, (b) H-Plane.

For example, tilt angles of $\theta = 0°$, $5°$, and $10^{\mathbf{0}}$ result in phase settings of 22.5°, 45°, and 67.5° for the first port,

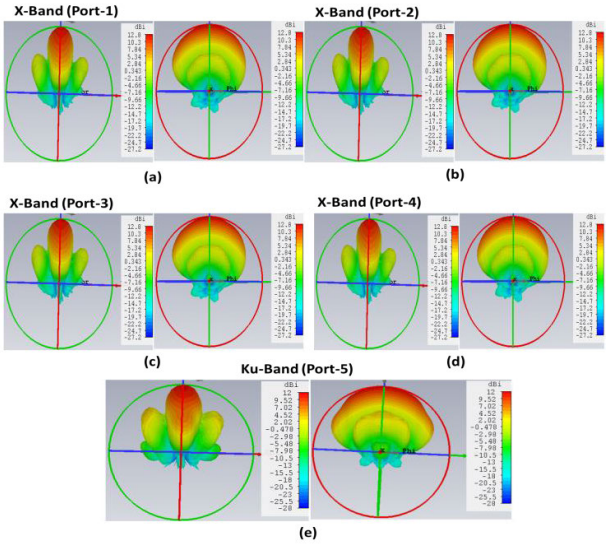

FIGURE 19. 3D Radiation patterns of Single-layer SAA design configuration at X/Ku-Band for port-1 (a) X-band- E-Plane, X-band-H-Plane (b) Port-2 X-band E-Plane, X-band H-Plane (c) Port-3 X-band E-Plane, X-band H-Plane (d) Port-4 X-band E-Plane, X-band H-Plane (e) Port-5 Ku-band E-Plane, Ku-band H-Plane.

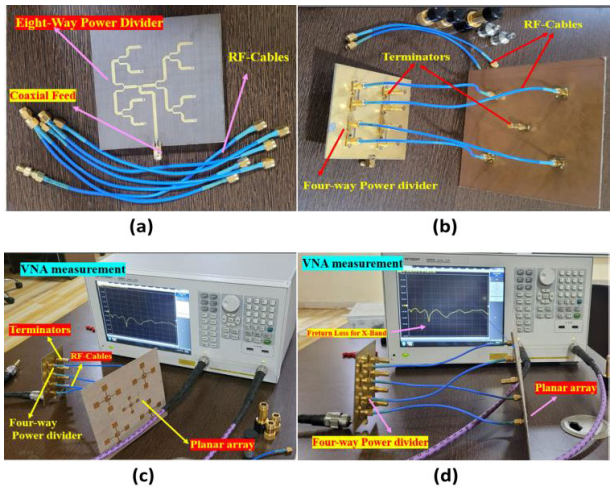

FIGURE 20. (a) Fabricated top view of power divider X-band (b) Bottom view of connected X/Ku-Band SAA (c) Measurement setup with vector network analyzer.(d) Measured return loss using four-way power divider for X-band.

respectively. Similarly, other tilt angles are achieved by adjusting the phases accordingly (e.g., $\theta = 10°$ with phases of 45°, 90°, and 135°). These different phase settings are illustrated in Figure 23. As an example, Figures 23 show the 3D beam patterns obtained using CST simulation by changing the phase excitation values of the four ports. By adjusting the phase values of the ports, the beam direction can be steered to different angles, allowing for beam scanning capability in the 2×2 planar array configuration.

To prove the concept of shared aperture antenna using a single layer the prototype has been developed and achieved reasonable electrical (S-parameters) and radiation

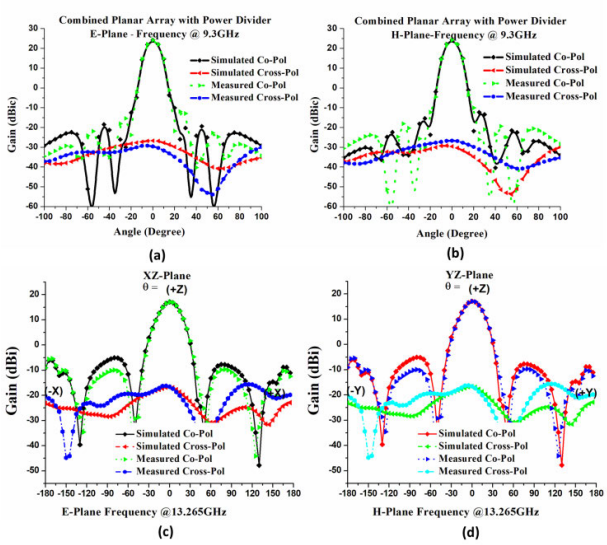

FIGURE 21. (a) Simulated and measured Co-Pol and cross Pol for XZ-Plane (E-Plane) (b) Simulated and measured Co-Pol and cross Pol for YZ-Plane (H-plane) Single-layer SAA design configuration at X/Ku-Band.

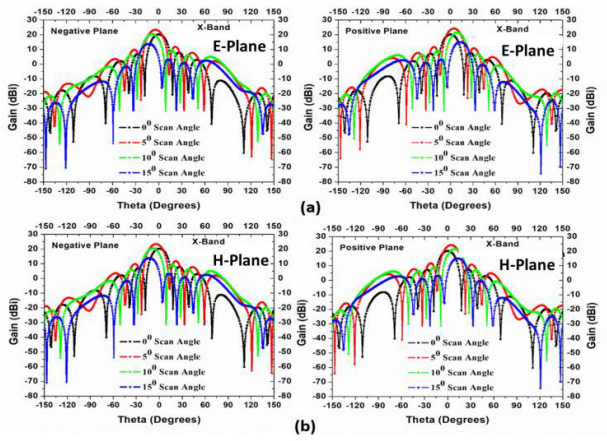

FIGURE 22. Scan angle patterns for different progressive phase shift (a) X-band E-plane. (b) X-band H-plane

characteristics in comparison with simulated and measured results. The summary of X/Ku-band SAA for both case-3 and case-4 has been given in Table 4.

Table 5 shows the comparison with other SAAs.Upon comparing the proposed antenna with the previous state-of-the-art works listed [11], [12], [14], [15], [16], [17], [19], [30], [31], [32], [36], [37], [38], [39], several key improvements can be observed. Firstly, the proposed antenna achieves a higher gain of 20 dBi and 12 dBi, surpassing the gains reported in the previous works. This signifies a notable advancement in signal strength and reception capability. Additionally, the proposed antenna demonstrates a significantly improved isolation of 67 dB. This indicates a reduced level of interference and better performance compared to the previous state-of-the-art antennas [11], [12], [14], [16], [17], [18], [19], [30], [31], [32], [33], [34], [35], [36], [38], [39], where lower isolation

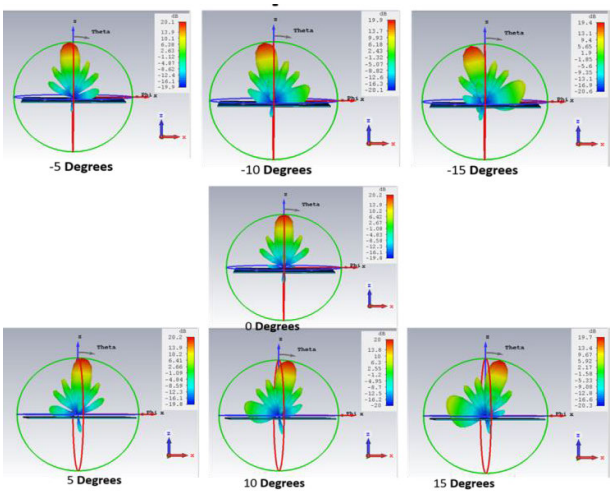

FIGURE 23. 3D far-field gain, elevation tilt angle ($\varphi = 0^0$ & $\theta = -5^0, -10^0$, and -15^0), broadside direction ($\varphi = 0^0$ & $\theta = 0^0$), Elevation tilt angle ($\varphi = 0^0$&$\theta = +5^0, +10^0, +15^0$).

values were reported. The higher isolation value achieved by the proposed antenna enhances its ability to reject unwanted signals and minimize interference between the bands. One of the most impressive achievements of the proposed antenna is its aperture efficiency of 93%. This surpasses the aperture efficiencies reported in the previous works [11], [12], [14], [15], [16], [17], [18], [19], [31], [32], [33], [34], [35], [36], [37], [38]. The higher aperture efficiency indicates a greater ability to capture and utilize incoming electromagnetic energy, resulting in improved overall antenna performance and effectiveness. Overall, the comparison highlights the superior performance of the proposed antenna in terms of gain, isolation, and aperture efficiency. These advancements signify the potential for enhanced signal reception, reduced interference, and improved overall functionality, positioning the proposed work as a significant development in the field of antenna design.

VI. DIRECTIONS OF IMPROVEMENT AND FUTURE SCOPE

Shared aperture antennas are designed to consolidate the functions of multiple antennas into a single unit. By utilizing wideband multiple beam technology, these antennas combine numerous antennas into a single aperture. This approach has proven beneficial in various applications, including airborne Synthetic Aperture Radar (SAR) systems. The design principles of shared aperture antennas can be adapted and modified to accommodate high-frequency ratios. For instance, a recommended design could involve the utilization of a Ku-band 5-element group with coaxial feeding, which can be integrated with a 5-element 4-group X-band planar array. Coaxial probe feeding is advantageous as it allows flexibility in placing the feed at any location inside the patch, ensuring optimal matching of the input. However, when working with thicker substrates, the length of the probe needs to be increased to counteract the inductive effect that arises, thus limiting the effectiveness of coaxial probe

TABLE 4. Summary of simulated and measured results for X-band 1 to 4-ports for Ku-band (port-5).

Operating Band		X-Band Simulated Group-1	X-Band Simulated Group-2	X-Band Simulated Group-3	X-Band Simulated Group-4	X-Band Measured Results from Group-1	X-Band Measured Results from Group-2	X-Band Measured Results from Group-3	X-Band Measured Results from Group-4	X-Band All Groups Combined With power divider/combiner	Operation Bands		Ku-Band Simulated Results Group-V	Ku-Band Measured Results Group-V
Centre Frequency		9.3 GHz	9.3 GHz	9.3 GHz	9.3 GHz	9.3 GHz	9.3 GHz	9.3 GHz	9.3 GHz	9.3 GHz	Centre Frequency		13.265 GHz	13.265 GHz
Polarization		linear	linear	linear	linear	linear	linear	linear	linear	linear	Polarization		Linear	Linear
Impedance bandwidth (MHz)		275(MHz)	275(MHz)	275(MHz)	275(MHz)	269(MHz)	269(MHz)	269(MHz)	269(MHz)	269(MHz)	Impedance bandwidth (MHz)		459(MHz)	459 (MHz)
Isolation		>50dB				>50dB				>50dB	Isolation		>60dB	
Antenna size(mm)		160mm×160mm×1.6 mm								Power divider externally connected with RF cables	Antenna size(mm)		160mm×160mm×1.6 mm	
Gain (dBi)		12.3	12.3	12.3	12.3	12	12	12	12	21	Gain(dBi)		11.6	11.3
Radiation Efficiency		93%	93%	93%	93%	92%	92%	92%	92%	90%	Radiation Efficiency		94%	92%
E-Plane	Cross-pol (dB)	-35	-35	-35	-35	-26	-26	-26	-26	-25	E-Plane	Cross-pol (dB)	-35	-29
	HPBW (deg)	80.5	80.5	80.5	80.5	78.5	78.5	78.5	78.5	16		HPBW (deg)	78.9	76.6
	SLL (dB)	-16	-16	-16	-16	-16.2	-16.2	-16.2	-16.2	-15		SLL (dB)	-16.8	-16.5
H-Plane	Cross-Pol (dB)	-21.7	-21.7	-21.7	-21.7	-19.5	-19.5	-19.5	-19.5	-20.1	H-Plane	Cross-Pol (dB)	-12	-12
	HPBW (deg)	22.2	22.2	22.2	22.2	23.4	23.4	23.4	23.4	12.6		HPBW (deg)	20.1	22.5
	SLL (dB)	-14	-14	-14	-14	-14.8	-14.8	-14.8	-14.8	-15		SLL (dB)	-13.9	-14.1

TABLE 5. Comparison with other shared aperture antennas.

S-No	Year	Band-1 /Band-2	Resonance Frequency GHz	Frequency ratio	Band-Width	configuration	Gain dBi	Cross-pol dB	Isolation dB	Aperture efficiency	Aperture size	Scan angle	Application
[11]	2018	X/Ku	11.2/13.5	1:1.2053	18.62%	Planar array 2×3	8.5	NA	40	90%	2.99×1.87×0.059 λ^3	$\pm25^0$	Radar Application
[12]	2011	L/S/X	1.25/3.5/10	1:2.8:2.8	13.4%/14.8%/16.8%	Planar array 16×2	22-21	30	37	62% 61.2%	NA	$\pm27^\circ$	Radar Application
[14]	2018	S/L	2-4/1-2	NA	6.9%/28.5%	Planar array 20×20	5/7.16	NA	40/45	92%	80×80×1.6mm^3	$\pm45^0$	Radar Application
[15]	2017	L/C	1.25/5.5	4.4	12.7%/16.8%	NA	12.9/26.8	-28/25 -28/28dB	NA	86%	NA	$\pm55^0$	Wireless Application
[16]	2017	S/X	2.5/8.2	1: 3.3.	13%	Planar array 2 × 2	7.5 dBi	NA	38	90%	NA	$\pm25^0$	Radar Application
[17]	2017	S/X	2.6-2.8/7.7-8.5	NA	7% /10.5%	NA	8 /11.5 dB	-18/-22dB	20 dB	91%	140 × 140 × 64 mm^3	$\pm25^0$	satellite applications.
[18]	2017	X/Ku/Ka	9.6, 14.8, and 34.5 GHz	1:1.8:4.5	3.6%, 6.7%, and 5.3%	Planar array	NA	-25 dB	<30	85%	NA	$\pm25^0$	SAR Application
[19]	2021	S/X	2.3-2.6/7.8-8.3	1:3.3	12.2%/6.2%	Planar array	7.4/10	-17	28/32	90%	NA	$\pm25^0$	SAR Application
[31]	2020	S/X	8.55 to 9.6	2.7:1.	11.7%	Multilayer 8 × 16	7.6 dBi	NA	35 dB	95%	NA	$\pm50^\circ$	Wireless Application
[32]	2021	Ku/Ka	14.2-18/31.0-33.6 GHz	2.1	14.2-18.0%	Multilayer Phased Array 2×3/4×4	8.4dbi/9dbi/8.7dbi	8.4dbi/9dB/8.7dB	15dB	86%	NA	$\pm25^0$	Wireless Application
[33]	2021	S/C	2.12-2.75/5.69-5.91	2.4	25.8%	Multilayer Phased Array 6 × 6	7.9dbi/2.7dbi/11.7dbi	7.9dbi/2.7dB/11.7dB	43/25 dB	86%	NA	$\pm25^0$	Satellite Communication
[34]	2022	Ku/Ka	13/38 GHz	2.9	25.0% 11.4%	Multilayer	28.2/37.2 dbi	28.2/37.2 dB	>30 dB	44.9% and 41.8%,	9.6 mm × 9.6 mm	$\pm25^0$	Satellite Communication
[35]	2022	S/C	2.4/5.8 GHz	2.4	43%	Multilayer 4×4	11.7 dbi	11.7 db	30 dB	61.6%	2.8 cm × 4.9 cm,	$\pm25^0$	Wireless Application
[36]	2022	Ku/Ka	16/35 GHz	2.2	25/11.4 %	Multilayer 8×8/8×8	22.3 dBi/22.1 dBi.	-22dB	>30 dB	86%	-	$35^0/40^0/50^0/60^0$	Satellite Communication
[37]	2022	S/L	3.4-3.8/0.69-0.96 GHz	2.1	3.4/3.8	Multilayer	7.3/13 db	>20/>15 dB	>30 dB/>25dB	89%	123×123×100	$\pm25^0$	future 5G Application
[38]	2023	Ka	28 GHz		30.62-27.51(3.11)	Single ayer1 × 4	9.56-dBi/8.9dBi	3.23 dB	32 dB	90%	22 × 4.1 × 1.97 mm3	$\pm45^\circ$	MIMO Application
[39]	2023	Ku/Ka	16 GHz /33.5 GHz	1.21	19.4% 7.4%	Multilayer 1 × 4	18.4/18 dBi 23.4/22.9 dBic	18.4/23.4 dB	15 dB	60/50	90.5×90.5×58.279	$\pm25^0$	Satellite Communication
[40]	2023	K/Ka	17.7–21.2 /27.5–31.0 GHz	1.5	18/12%	Multilayer	4.5dBi	4.5dB	40dB	NA	NA	$\pm60^0$	LEO Satellite Communication
This work		X/Ku	9.3/13.265	1:1.4263	276/459MHz	Planar array (Single Layer)	22.3/12.8	-16.5/-18	>50dB	93%	160×160×1.6mm^3	$\pm25^0$	SAR Application

feeding in such cases. The advancement of airborne and spaceborne sensors has significantly improved SAR capabilities, enabling the acquisition of high-quality SAR data with decimeter resolution. This breakthrough has opened up new avenues for data analysis and information extraction. The combination of higher spatial resolution and novel imaging modalities has played a vital role in achieving these advancements.

VII. CONCLUSION

A novel dual-band single-polarized (DBSP) high gain shared aperture antenna (SAA) with better isolation is proposed for the use in Airborne Synthetic Aperture Radars (AIR-SARs). To validate the antenna design, a prototype is fabricated and tested for S-parameters, radiation characteristics, and gain measurements. The antenna with return loss of S11 < -10 dB has an impedance bandwidth (BW) (9.1919-9.4674 GHz) (276 MHz with 2.96% BW) in X-band and (13.054-13.513 GHz) (459 MHz with 3.46% BW) in Ku-band. More than 25 dB of isolation has been measured between S_{21} $=S_{12}$ for case 3 and are >35dB isolation between in-band ports (P12/P23/P13) for case 4. Additionally, it achieves high gain values of 12.8 dBi for the X-band and 12 dBi for the Ku-band for case 3. The 2 × 2 planar array (5-elements in each group excited with coaxial probe feed) is connected with 8-way power divider (4-groups are feed with 4 power divider ports and other 4-ports are matched with 50Ω terminations) and achieved a gain of 19 dBi for the X-band and 12 dBi for the Ku-band for case 4. The combined gain was varied between 19dBi to 20dBi with 0^0 to 25^0 scan angle. The combined 2 × 2 planar x-band array Half-Power Beam width (HPBW) values are 16° in the E-plane and 12.6° in the H-plane for the X-band, while for the Ku-band, they are 22.7° in the E-plane and 78.4° in the H-plane. The size of the shared-aperture antenna is 160 mm × 160 mm × 1.6 mm. The proposed SAA is ideal for soil moisture estimation in agricultural areas and suitable for applications in snow-covered regions, cold areas, and disaster monitoring. Finally the present reported SAA X/Ku-DBSP holds significant value for AIR-SAR applications.

ACKNOWLEDGMENT

The authors would like to thank Rogers Corporation, USA, for their support in providing RT Duroid 5880 samples for academic research purposes, also would like to thank the Junior Assistant, Ravi Kumar Dasari (for his support during fabrication and assembling), Department of Electronics Communication Engineering (ECE), School of Electrical, Electronics, and Communication Engineering, Vignan's Foundation for Science, Technology, and Research (Deemed to be University), Vadlamudi, Guntur, Andhra Pradesh, India, and also would like to thank the reviewers of the manuscript. Dr. Venkata Kishore Kothapudi would like to thank the Director Dr. Ravi Sekhar Yarrabothu and the In-charge Dr. Pachiyaannan Muthusamy of their COE for their tremendous support in facilitating the timely requirements for completing this research work. This work has been carried out with the Centre of Excellence Advanced RF Microwave & Wireless Communications.

REFERENCES

[1] A. Moreira, P. Prats-Iraola, M. Younis, G. Krieger, I. Hajnsek, and K. P. Papathanassiou, "A tutorial on synthetic aperture radar," *IEEE Geosci. Remote Sens. Mag.*, vol. 1, no. 1, pp. 6–43, Mar. 2013, doi: 10.1109/MGRS.2013.2248301.

[2] A. Javali, J. Gupta, and A. Sahoo, "A review on synthetic aperture radar for Earth remote sensing: Challenges and opportunities," in *Proc. 2nd Int. Conf. Electron. Sustain. Commun. Syst. (ICESC)*, Aug. 2021, pp. 596–601, doi: 10.1109/ICESC51422.2021.9532910.

[3] V. K. Kothapudi and V. Kumar, "SFCFOS uniform and Chebyshev amplitude distribution linear array antenna for K-band applications," *J. Electromagn. Eng. Sci.*, vol. 19, no. 1, pp. 64–70, Jan. 2019, doi: 10.26866/jees.2019.19.1.64.

[4] D. M. Pozar and D. H. Schaubert, "Comparison of three series fed microstrip array geometries," in *Proc. IEEE Antennas Propag. Soc. Int. Symp.*, Jun. 1993, pp. 728–731, doi: 10.1109/APS.1993.385244.

[5] T. Yuan, N. Yuan, and L.-W. Li, "A novel series-fed taper antenna array design," *IEEE Antennas Wireless Propag. Lett.*, vol. 7, pp. 362–365, 2008, doi: 10.1109/LAWP.2008.928487.

[6] F.-Y. Kuo and R.-B. Hwang, "High-isolation X-band marine radar antenna design," *IEEE Trans. Antennas Propag.*, vol. 62, no. 5, pp. 2331–2337, May 2014, doi: 10.1109/TAP.2014.2307296.

[7] V. K. Kothapudi and V. Kumar, "A single layer S/X-band series-fed shared aperture antenna for SAR applications," *Prog. Electromagn. Res. C*, vol. 76, pp. 207–219, 2017, doi: 10.2528/PIERC17070104.

[8] S. Karimkashi and G. Zhang, "A dual-polarized series-fed microstrip antenna array with very high polarization purity for weather measurements," *IEEE Trans. Antennas Propag.*, vol. 61, no. 10, pp. 5315–5319, Oct. 2013, doi: 10.1109/TAP.2013.2273813.

[9] C. Deng, P. Li, and W. Cao, "A high-isolation dual-polarization patch antenna with omnidirectional radiation patterns," *IEEE Antennas Wireless Propag. Lett.*, vol. 11, pp. 1273–1276, 2012, doi: 10.1109/LAWP.2012.2226555.

[10] V. K. Kothapudi and V. Kumar, "Compact 1 × 2 and 2 × 2 dual polarized series-fed antenna array for X-band airborne synthetic aperture radar applications," *J. Electromagn. Eng. Sci.*, vol. 18, no. 2, pp. 117–128, Apr. 2018, doi: 10.26866/jees.2018.18.2.117.

[11] M. Alibakhshikenari, B. S. Virdee, C. H. See, R. A. AbAlhameed, F. Falcone, and E. Limit, "Array antenna for synthetic aperture radar operating in X and Ku-bands: A study to enhance isolation between radiation elements," in *Proc. 12th Eur. Conf. Synth. Aperture Radar*, 2018, pp. 1–5.

[12] S.-S. Zhong, Z. Sun, L.-B. Kong, C. Gao, W. Wang, and M.-P. Jin, "Design of TBDP shared-aperture SAR array," in *Proc. Asia–Pacific Microw. Conf.*, Dec. 2011, pp. 159–162.

[13] H. Saeidi-Manesh and G. Zhang, "High-isolation, low cross-polarization, dual-polarization, hybrid feed microstrip patch array antenna for MPAR application," *IEEE Trans. Antennas Propag.*, vol. 66, no. 5, pp. 2326–2332, May 2018, doi: 10.1109/TAP.2018.2811780.

[14] J. Dhiman, A. Sharma, and S. K. Khah, "Shared aperture microstrip patch antenna array for L and S-bands," *Prog. Electromagn. Res. Lett.*, vol. 86, pp. 91–95, 2019, doi: 10.2528/PIERL19052905.

[15] Z. Sun, K. P. Esselle, S.-S. Zhong, and Y. J. Guo, "Shared-aperture dual-band dual-polarization array using sandwiched stacked patch," *Prog. Electromagn. Res. C*, vol. 52, pp. 183–195, 2014.

[16] P. Mathur and G. Kumar, "Antenna at S-band as ground for array at X-band in dual frequency antenna at S/X-bands," *Prog. Electromagn. Res. Lett.*, vol. 71, pp. 15–22, 2017.

[17] P. Mathur and G. Kumar, "Dual-frequency microstrip antenna at S and X bands with higher-order mode suppression technique," *IET Microw., Antennas Propag.*, vol. 12, no. 4, pp. 583–587, Mar. 2018, doi: 10.1049/iet-map.2017.0224.

[18] P. Mathur and G. Kumar, "Dual-band dual-polarized microstrip antenna at S- and X-bands using feed technique for suppression of interference due to higher order modes," *Int. J. RF Microw. Comput.-Aided Eng.*, vol. 31, no. 11, Nov. 2021, doi: 10.1002/mmce.22870.

[19] C.-X. Mao, S. Gao, Q. Luo, T. Rommel, and Q.-X. Chu, "Low-cost X/Ku/Ka-band dual-polarized array with shared aperture," *IEEE Trans. Antennas Propag.*, vol. 65, no. 7, pp. 3520–3527, Jul. 2017, doi: 10.1109/TAP.2017.2700161.

[20] A. Doerry, "Introduction to synthetic aperture radar," in *Proc. IEEE Radar Conf. (RadarConf)*, Apr. 2019, pp. 1–90, doi: 10.1109/RADAR.2019.8835560.

[21] P. A. Rosen, S. Hensley, I. R. Joughin, F. K. Li, S. N. Madsen, E. Rodriguez, and R. M. Goldstein, "Synthetic aperture radar interferometry," *Proc. IEEE*, vol. 88, no. 3, pp. 333–382, Mar. 2000, doi: 10.1109/5.838084.

[22] A. Freeman, M. Zink, E. Caro, A. Moreira, L. Veilleux, and M. Werner, "The legacy of the SIR-C/X-SAR radar system: 25 years on," *Remote Sens. Environ.*, vol. 231, Sep. 2019, Art. no. 111255, doi: 10.1016/j.rse.2019.111255.
[23] B. Walker, G. Sander, M. Thompson, B. Burns, R. Fellerhoff, and D. Dubbert, "A high-resolution, four-band SAR testbed with real-time image formation," in *Proc. Int. Geosci. Remote Sens. Symp.*, 1996, pp. 1881–1885, doi: 10.1109/IGARSS.1996.516827.
[24] Q. Li, D. Perissin, Q. Luo, H. Lin, and M. Pang, "High resolution SAR change detection in Hong Kong," in *Proc. IEEE Int. Geosci. Remote Sens. Symp.*, Jul. 2011, pp. 1630–1633, doi: 10.1109/IGARSS.2011.6049544.
[25] F. Daum, "Radar handbook, 3rd edition (M.I. Skolnik, Ed; 2008) [book review]," *IEEE Aerosp. Electron. Syst. Mag.*, vol. 23, no. 5, p. 41, May 2008, doi: 10.1109/MAES.2008.4523916.
[26] E. M. R. Storvold, "Snow covered area retrieval using Envisat ASAR wideswath in mountainous areas," in *Proc. IEEE Int. Geosci. Remote Sens. Symp.*, Sep. 2004, pp. 1845–1848, doi: 10.1109/IGARSS.2004.1370697.
[27] H. A. Hovland, J. A. Johannessen, and G. Digranes, "Slick detection in SAR images," in *Proc. IEEE Int. Geosci. Remote Sens. Symp.*, Aug. 1994, pp. 2038–2040, doi: 10.1109/IGARSS.1994.399647.
[28] M. R. Drinkwater, R. Kwok, and E. Rignot, "Synthetic aperture radar polarimetry of sea ice," in *Proc. 10th Annu. Int. Symp. Geosci. Remote Sens.*, May 1990, pp. 1525–1528, doi: 10.1109/IGARSS.1990.688793.
[29] B. Chen, M. Yang, Y. Wang, X. Dang, and B. Wu, "The applications and future of synthetic impulse and aperture radar," in *Proc. CIE Int. Conf. Radar*, 2016, pp. 1–5.
[30] C. Zhou, S. Yuan, H. Li, B. Wang, and H. Wong, "Dual-band shared-aperture antenna with bifunctional metasurface," *IEEE Antennas Wireless Propag. Lett.*, vol. 20, no. 10, pp. 2013–2017, Oct. 2021, doi: 10.1109/LAWP.2021.3102104.
[31] Y. Liu, Y. J. Cheng, and Y. Fan, "A dual-layer Ku/Ka dual-band shared-aperture reflectarray antenna based on structure-reuse technique," in *Proc. IEEE Int. Symp. Antennas Propagation USNC-URSI Radio Sci. Meeting (APS/URSI)*, Dec. 2021, pp. 1925–1926, doi: 10.1109/APS/URSI47566.2021.9704250.
[32] C. X. Bai, Y. J. Cheng, Y. R. Ding, and J. F. Zhang, "A metamaterial-based S/X -band shared-aperture phased-array antenna with wide beam scanning coverage," *IEEE Trans. Antennas Propag.*, vol. 68, no. 6, pp. 4283–4292, Jun. 2020, doi: 10.1109/TAP.2020.2970096.
[33] L. Y. Liu, Y. J. Cheng, and L. Wang, "Dual-polarized Ku-band and single-polarized Ka-band shared-aperture phased array antenna," in *Proc. Int. Conf. Microw. Millim. Wave Technol. (ICMMT)*, May 2021, pp. 1–3, doi: 10.1109/ICMMT52847.2021.9618073.
[34] Y. R. Ding, Y. J. Cheng, J. X. Sun, L. Wang, and T. J. Li, "Dual-band shared-aperture two-dimensional phased array antenna with wide bandwidth of 25.0% and 11.4% at Ku- and Ka-band," *IEEE Trans. Antennas Propag.*, vol. 70, no. 9, pp. 7468–7477, Sep. 2022, doi: 10.1109/TAP.2022.3146867.
[35] W. Niu, B. Sun, G. Zhou, and Z. Lan, "Dual-band aperture shared antenna array with decreased radiation pattern distortion," *IEEE Trans. Antennas Propag.*, vol. 70, no. 7, pp. 6048–6053, Jul. 2022, doi: 10.1109/TAP.2022.3161267.
[36] J.-H. Ou, B. Xu, S. F. Bo, Y. Dong, S.-W. Dong, J. Tang, and X. Y. Zhang, "Highly-isolated RF power and information receiving system based on dual-band dual-circular-polarized shared-aperture antenna," *IEEE Trans. Circuits Syst. I, Reg. Papers*, vol. 69, no. 8, pp. 3093–3101, Aug. 2022, doi: 10.1109/TCSI.2022.3173688.
[37] B. Kim, M. Kim, D. Lee, J. Lee, Y. Youn, and W. Hong, "A shared-aperture cavity slot antenna-in-package concept featuring end-fire and broadside radiation for enhanced beam coverage of mmWave mobile devices," *IEEE Trans. Antennas Propag.*, vol. 71, no. 2, pp. 1378–1390, Feb. 2023, doi: 10.1109/TAP.2023.3234162.
[38] J. Ran, Y. Wu, C. Jin, P. Zhang, and W. Wang, "Dual-band multipolarized aperture-shared antenna array for Ku-/Ka-band satellite communication," *IEEE Trans. Antennas Propag.*, vol. 71, no. 5, pp. 3882–3893, May 2023, doi: 10.1109/TAP.2023.3248445.
[39] R. S. Hao, J. F. Zhang, S. C. Jin, D. G. Liu, T. J. Li, and Y. J. Cheng, "K-/Ka-band shared-aperture phased array with wide bandwidth and wide beam coverage for LEO satellite communication," *IEEE Trans. Antennas Propag.*, vol. 71, no. 1, pp. 672–680, Jan. 2023, doi: 10.1109/TAP.2022.3222091.
[40] (2018). *Computer Simulation Technology Version*. Wellesley-Hill, Wellesley, MA, USA. [Online]. Available: www.cst.com
[41] *Rogers Corporation*. [Online]. Available: www.rogerscorp.com

PRAVEENA KATI (Graduate Student Member, IEEE) was born in Guntur, India, in 1979. She received the degree in electronics and communication engineering from CIET, ANU, Lam, Guntur, India, in 2011, and the M.Tech. degree in communication and signal processing from LITAM, JNTUK, Dhulipalla, India, in 2013. She is currently pursuing the Ph.D. degree with the Microwave Division, Center of Excellence Advanced RF Microwave & Wireless Communications, Department of Electronics and Communication Engineering, School of Electrical, Electronics and Communication Engineering, VFSTR Deemed to be University, Vadlamudi, India. She has over seven years of an Assistant Professor experience in electronics and communication engineering with the Chalapathi Institute of Technology (CIT), Mothadaka. She has an experience in radar systems design, which includes transmitting/receiving modules [HF-, VHF-, C-, X-, and Ku-band], RF and microwave feeder network and beam forming, RF and microwave active and passive components, RF power amplifiers, and antenna systems, which includes the microstrip patch antennas as a linear array and phased array with different configurations by using analysis and synthesis techniques. She has published over seven research papers in international journals and national and IEEE international conferences. She has authored or coauthored many IEEE proceeding papers. Her research interests include shared aperture antenna technology (single layer -C/X/Ku-bands) for radar engineering, including airborne and space-borne synthetic aperture radar and radar wind profilers.

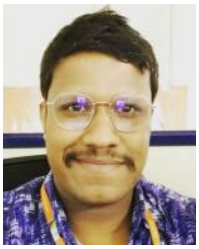

VENKATA KISHORE KOTHAPUDI (Senior Member, IEEE) was born in Tenali, Guntur, Andhra Pradesh, India, in 1987. He received the Graduate degree in electronics and communication engineering from TPIST, JNTU Hyderabad, India, in 2008, the M.Tech. degree in communication and radar systems from KLEF, India, in 2012, and the Ph.D. degree from the Microwave Division, School of Electronics Engineering (SENSE), Vellore Institute of Technology (VIT), Vellore, Tamil Nadu, India. He is currently an Associate Professor with the Department of Electronics and Communication Engineering, School of Electrical, Electronics and Communication Engineering, Vignan's Foundation for Science, Technology, and Research (VFSTR), Vadlamudi, Guntur, Andhra Pradesh, India. He has published more than 20 research papers in international journals and national and IEEE international conferences. He has been the author or coauthor of many IEEE proceeding papers. He has published research papers in IEEE Access, with a 3.557 impact factor, *IET Microwave, Antennas & Propagation*, the *Progress in Electromagnetic Research* (PIER), *Journal of Electromagnetic Engineering and Science* (JEES), and IEEE international conferences. He is a Reviewer of several reputed journals (IEEE Access, IET journals, *Electronics Letters*, *IJCS* (Wiley), Springer journals, *JEES*, Applied Computational Electromagnetics Society, *Advanced Electromagnetics*, and *JESTR*). He travelled to Sri Lanka and Singapore for the IEEE SYWC 2015 Meeting and the IEEE APSAR 2015 Conference, respectively, to present his research work and as a part of his research. He has more than ten years of academics, research and industry experience in RF and microwave engineering in ECIL as a GEA and NARL-ISRO as a Project Student and Astra Microwave Products as an Engineer. He has a rich experience on radar systems design which includes transmit/receive modules (HF, VHF, L, and S & C-Band), RF & microwave feeder network and beam forming, RF & microwave active and passive components, RF power amplifiers, and antenna system which includes Yagi-Uda and microstrip patch antenna as a phased array with different configurations by using analysis and synthesis techniques. His research interests include shared aperture antenna technology (single layer and multilayer-L/S/C/X/K-bands) for radar engineering includes airborne and space borne synthetic aperture radar and radar wind profilers. He is a Senior Member of the American Institute of Aeronautics and Astronautics (AIAA) and ACES. He is associated with IEEE societies (AP-s., MTT-s., AES-s., GRS-s., IP-s., ComSoc, and EMC-s.).